

**Part One**  
**Spectroscopic Methods for Nano Interfaces**



## 1

## Raman and Fluorescence Spectroscopy Coupled with Scanning Tunneling Microscopy

*Noriko Nishizawa Horimoto and Hiroshi Fukumura*

## 1.1

### Introduction

Optical spectroscopy is a very powerful tool in many fields, especially in chemistry. Light irradiates molecules (input) and, after interaction with the molecules, light is collected (output). In Raman spectroscopy, light is inelastically scattered by molecules and, owing to molecular vibration excitation or de-excitation, light with higher or lower energy is observed. Raman scattering is emitted together with a vast amount of elastically scattered light known as Rayleigh scattering, which generally makes the measurement of Raman spectra difficult. Raman spectra are, however, very valuable because we can obtain directly the vibration frequencies of bonds contained in matter by using visible light. In fluorescence spectroscopy, light is absorbed by molecules and the molecules are excited to the electronically excited state, resulting in the emission of fluorescence when the molecules relax to the ground state. Fluorescence spectra and decay processes are generally sensitive to intermolecular interactions in excited states. By the use of such optical spectroscopy, chemical species can be identified and the average environment surrounding target molecules can be deduced.

Conventional optical spectroscopy has the drawback that the spatial resolution is limited because of the diffraction limit of light. The resolution of a conventional microscope is about half of the observation wavelength, which is several hundred nm in the case of visible light. A variety of attempts to overcome the diffraction limit realizing better spatial resolution have been performed to date. Scanning near-field optical microscopy (SNOM) is one such methods, which has a spatial resolution of about 50 nm [1]. In aperture SNOM, light is irradiated from a tapered optical fiber tip so that the spatial resolution is limited by the aperture. Aperture-less SNOM uses a sharp tip which scatters the evanescent field containing the information in the sub-wavelength range. In both types of SNOM, the tip is placed close to or in contact with a sample, and light signals are collected while the tip scans the sample surface.

The combination of atomic force microscopy (AFM) and Raman spectroscopy is another approach to attain high spatial resolution. AFM also employs a sharp tip close to a sample surface. When the tip is made of metal and light is irradiated onto the tip and surface, Raman scattering is largely enhanced. In this way, a spatial resolution of 15 nm is achieved [2].

However, there is demand for better spatial resolution – ultimately atomic scale resolution. If this is realized we will be able to distinguish individually molecules densely packed on a surface, or even identify a part of a single molecule. For example, it could be clarified which part of a large molecule is modified with which kind of functional group. This kind of instrument may become essential for the preparation and analysis of single molecular devices. Combining scanning tunneling microscopy (STM) with optical spectroscopy is considered to be a feasible approach. This is because, at present, STM has the highest resolution among the various types of scanning probe microscopy. STM was developed by Binnig *et al.* in 1982 [3], and now enables us to observe a sample surface with atomic-scale resolution. The principle of the method is based on the tunneling current between the sample and a sharp metal tip as a tunneling probe [4, 5]. Very recently, attempts to combine STM with Raman or fluorescence spectroscopy have emerged and these will be described in this chapter. Here we will focus on studies performed under ambient conditions, that is, at room temperature and in air. Therefore, inelastic electron tunneling STM spectroscopy (IETS) is omitted from this chapter. STM induced luminescence, (alternatively called photon scanning tunneling microscopy, PSTM) which observes the luminescence induced by the STM tunneling current, is also beyond the scope of this chapter.

## 1.2

### Outline of STM Combined with Optical Spectroscopy

#### 1.2.1

##### Raman Spectroscopy

STM-Raman spectroscopy utilizes the effect that Raman scattering is enhanced for a molecule in the vicinity of a metal nanostructure. This enhancement effect is generally called surface-enhanced Raman scattering (SERS). When a sharp scanning probe, such as a tunneling tip for STM, is used as a metal nanostructure to enhance Raman intensity, it is called “tip-enhanced Raman scattering” (TERS). The concept of STM combined with Raman spectroscopy is presented in Figure 1.1.

The mechanisms of surface enhanced Raman scattering have been well discussed in the early review papers [6, 7]. Briefly, Raman enhancement is considered to occur by two mechanisms: chemical enhancement and electromagnetic enhancement. The chemical enhancement is due to resonance Raman scattering based on charge transfer between a metal nanostructure and a molecule, and takes place only when the metal nanostructure is in contact with the molecule. In STM, the tip is close to the sample molecule but not close enough to induce charge transfer, so the enhancement by the chemical effect may be negligibly small. The electromagnetic enhancement

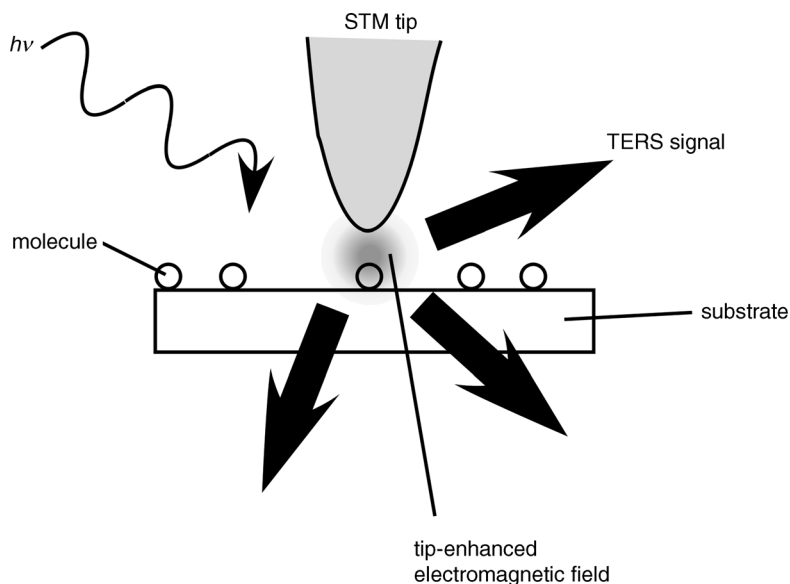


**Figure 1.1** Concept of STM combined with Raman spectroscopy.

arises from the field enhancement in the vicinity of a metal nanostructure when it is illuminated by probe light. This is due to the excitation of localized surface plasmons in the metal nanostructure, which is a collective oscillation of the electron gas at the subsurface of the metal. The enhancement factor of Raman intensity is roughly proportional to  $M^4$ , where  $M$  is the factor indicating by how much the electric field is enhanced by the nanostructure, since both the incident light intensity and the scattered light intensity are enhanced [8, 9]. The enhancement factor is especially large when the nanostructure is made of silver, gold, or other metals containing free electrons. By changing the shape, size, or material of the metal nanostructure, and the surrounding medium, the wavelength dependence of the enhancement efficiency changes due to changes in plasmon resonance. The optical response of metal nanospheres can be described precisely by using the Mie theory, which is an analytical solution of Maxwell's equation. Its details and numerical calculation programs are fully and comprehensively presented by Bohren and Huffman [10]. For non-spherical particles, numerical approximation methods are generally required. The finite different time domain (FDTD) method [11], and the discrete dipole approximation (DDA) [12, 13] are commonly utilized. For a classical SERS substrate, which is a roughened silver electrode, the average enhancement factor is known to be about  $10^6$  [14]. For a selected single silver nanoparticle with a single molecule, the enhancement factor is reported to be  $10^{14}$  [15]. A maximum enhancement factor of about  $5 \times 10^9$  is reported for TERS [16]. It should be noted that the net enhancement factor by TERS is large but the observed signal increase is sometimes small because the spot having the intense electric field under a tunneling tip is very limited compared with the area illuminated by the probe light beam.

## 1.2.2

**Fluorescence Spectroscopy**

The effect of a tunneling tip on fluorescence is rather complicated compared with that on Raman scattering. The enhancement of the electric field is induced by approaching the metal tip to a fluorescent molecule; however, the quenching of fluorescence is also caused in the vicinity of or in contact with the surface of the metal. Generally, four major processes in fluorescent molecules are known to compete with the emissive decay: energy transfer, electron transfer, intersystem crossing, and internal conversion. Energy transfer can take place when an energy acceptor comes as close as about 5 nm to a fluorescent molecule, depending on the interaction between the excited state of the molecule and the ground state of the acceptor. Here the energy acceptor can be the nanostructured metal tip which shows an absorption spectrum in the visible region. The interaction is roughly estimated from the overlap of the molecular fluorescence and the acceptor absorption spectra. When the metal tip approaches to less than 1 nm from the fluorescent molecule, strong interactions like electron transfer and electron exchange can occur, which results in the fast decay of excited states. Intersystem crossing to triplet states is also known to be accelerated by approaching heavy atoms to fluorescent singlet states. This is caused by the enhancement of spin-orbit coupling, which requires the overlap of electron orbitals. Although internal conversion is rather intrinsic to molecular electronic states, it may be affected by approaching a metal tip if the vibronic coupling in a fluorescent molecule is modified through the molecular structure distortion. Thus, there are plural processes reducing fluorescence intensity, in addition to the electromagnetic field enhancement effect. Roughly speaking, the enhancement effect extends to 10 nm or more around the tunneling tip although the quenching effects become dominant only at a few nm from the tip, which results in a donut-like enhancement pattern for fluorescence.

## 1.3

**Theoretical Approaches**

Demming *et al.* calculated the field enhancement factor (FEF) for a silver tip and a flat gold surface by the boundary element method [17]. They demonstrated that the peak position and the magnitude of the FEF maximum depend on the geometry of the tip. For smaller tip radii, the FEF maximum increases and shifts to longer wavelength. The wavelength dependence of the FEF for a silver ellipsoid also behaves in this manner when its aspect ratio is changed. The spatial distribution of the FEF also becomes narrower and the peak intensity becomes stronger when the tip shape becomes sharper. The same research group calculated the FEF for a small spheroid shape as a model of tips made of gold, platinum, silver, p-doped silicon, and tungsten, by solving the Laplace equation analytically [18]. They calculated the dependence of FEF on the aspect ratio of the ellipsoid and wavelength, as shown in Figure 1.2. They also calculated the FEF space distribution for a tip with a flat shape by a boundary

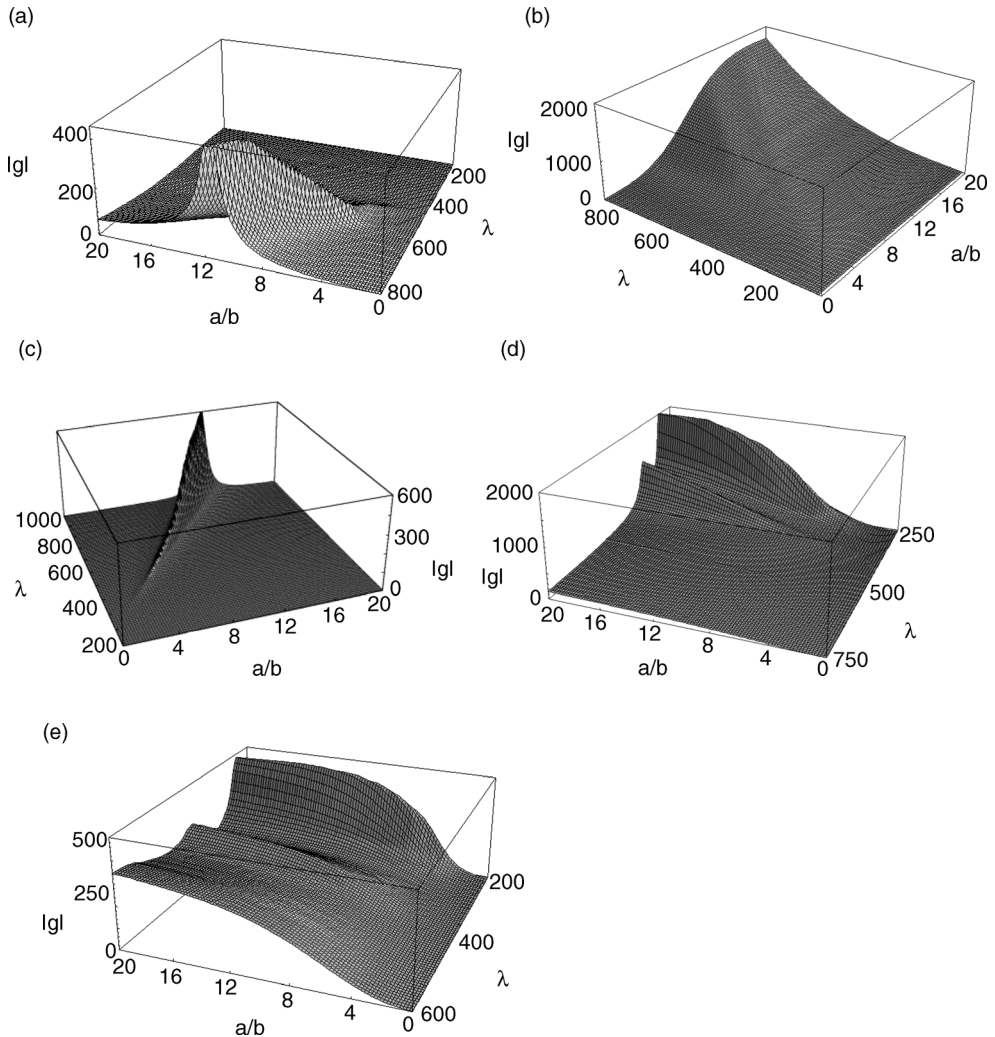


**Figure 1.2** Modulus of the field enhancement factor versus the aspect ratio  $a = b$  and wavelengths  $\lambda$  for SPM tips of different materials: (a) gold, (b) platinum, (c) silver, (d) p-doped silicon, (e) tungsten. Reprinted with permission from J. Jersch, *Applied Physics A*, 66, 29 (1998). Copyright 1998, Springer-Verlag.

element method. The intensity showed a double peak. These FEF calculation results were consistent with interesting experimental results: a flat Au surface was topographically changed to form a double structure by the illumination of the surface and a flat-shaped tip with laser light.

Mills calculated the enhancement of dynamic dipole moments for a dipole moment on a smooth silver or copper surface with a silver tip above it, which

leads to fluorescence enhancement and TERS [19]. They used a sphere as a model of the tip and calculated the enhancement factors for various wavelengths. It was found that the enhancement factors are larger for a dipole moment oriented perpendicular to the surface than for one oriented parallel to the surface and are also larger when the tip-sample distance is small. Using the same condition and a similar method, Wu and Mills performed calculations of the enhancement factors for various wavelengths for several tip-sample distances [20]. They also calculated the enhancement factor for dipoles at different lateral distances from directly beneath the tip. They confirmed that the lateral resolution scales as  $(RD)^{1/2}$ , with  $R$  the radius of curvature of the tip, and  $D$  its distance from the substrate, as was first suggested by Rendell *et al.* [21].

Klein *et al.* used the same model as Demming *et al.* [17], and calculated the FEF for an Ag tip near an Au surface [22], which is similar to the experimental conditions of Pettinger *et al.* [23]. They showed that Raman signals of molecules below or in the near field of the tip can be enhanced to practically measurable levels, and the FEF is larger for smaller tip-sample gaps, being localized below the tip, as shown in Figure 1.3.

Downes *et al.* calculated the enhancement of the scattered light intensity for a tip over a substrate using finite element electromagnetic simulations [24]. A gold tip or silicon tip over a gold, mica, or silicon substrate in air or water was considered. They calculated the enhancement dependence on incident light polarization, wavelength, tip-substrate separation, Raman shift, distance beneath the tip apex, angle between the tip axis and incident radiation, tip radius, and lateral displacement from the tip apex. The enhancement exceeded  $10^{12}$  or  $10^8$  for a 20 nm radius Au tip over an Au or mica substrate, respectively, for a tip-substrate separation of 1 nm. In both cases, the enhancement gradually decreased as the tip-substrate separation increased. They showed that with this enhancement, high-speed (10 ms integration time) mapping is possible considering the signal contrast against the far-field signal. The lateral resolution dependence on tip-substrate separation was also calculated, and the lateral resolution was better than 1 nm for a 10 or 20 nm radius Au tip over an Au substrate. The lateral resolution became worse as the tip-substrate separation increased.

## 1.4

### Experimental Approaches

#### 1.4.1

##### STM Combined with Raman Spectroscopy

Pettinger *et al.* observed a TERS spectrum of monolayer-thick brilliant cresyl blue (BCB) adsorbed on a smooth Au film surface by using a Ag tip, while no STM image of the adsorbed surface was shown [23]. The Raman intensity increased when the tip was in the tunneling position, meaning that the tip-surface distance was around 1 nm. They calculated the field enhancement factor by the method described by

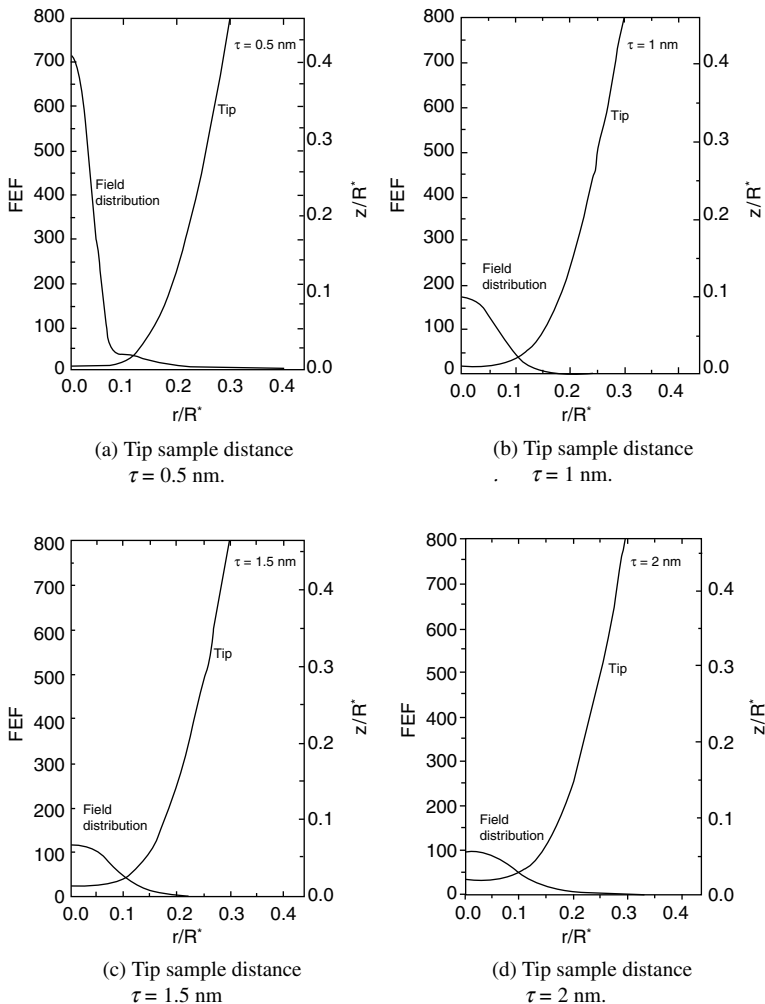


**Figure 1.3** Field distributions along the Ag-tip surface and corresponding Ag-tip geometry.  $z = 0$  corresponds to the Au-substrate.  $r/R^*$  is the normalized radius from the point directly beneath the tip ( $R^*$  is the Rayleigh length  $R^* = \lambda/2\pi$ ). Reprinted with permission from S. Klein, *Electrochemistry*, 71, 114 (2003). Copyright 2003, The Electrochemical Society of Japan.

Demming *et al.* [17], and compared it with their experimental results. The observed increase in Raman intensity by a factor of 15 within the laser focus of about  $2 \mu\text{m}$ , corresponds to a maximum local enhancement at the center of the tip apex by a factor of about 12 000 under the assumption that the tip radius is 100 nm. More precisely, about 20% of the Raman intensity is considered to originate from an area with a radius of 14 nm under the tip, which is roughly equivalent to 400 molecules out of  $2 \times 10^6$  in the total focused area.

Pettinger *et al.* further reported the TERS spectra of  $\text{CN}^-$  and BCB on a smooth and rough Au substrate with a silver tip [25]. They observed a signal enhancement by a factor of 4 for  $\text{CN}^-$ , and estimated the real enhancement to be at least three orders of magnitude, assuming the laser spot size to be  $2\ \mu\text{m}$ , and the tip radius at the apex to be  $100\ \text{nm}$ . They also observed TERS spectra of  $\text{CN}^-$  ions on SERS active Au surfaces [26], and compared the experimental result of the illumination from the bottom through a thin metal film with that of direct excitation from the top at an incident angle of  $60^\circ$ . It was found that subtraction of the SERS spectra from the TERS spectra shows narrow bandwidth spectra, suggesting that the TERS signal arises from a rather small amount of molecules.

Ren *et al.* reported a method to prepare a gold tip with a tip apex radius of  $30\ \text{nm}$  reproducibly [27]. They observed the TERS of a Malachite Green isothiocyanate (MGITC) monolayer on an Au(111) surface and obtained an enhancement factor of about  $1.6 \times 10^5$ , by using the relation,  $q = I_{\text{TERS}}/I_{\text{RRS}} = g^4 a^2 / R_{\text{focus}}^2$ , where  $q$  is the net increase in the signal,  $I_{\text{TERS}}$  and  $I_{\text{RRS}}$  are the signal intensities for TERS and RRS (resonance Raman scattering), respectively;  $g^4$  is the TERS enhancement ( $g$  is the field enhancement),  $a$  denotes the radius of the enhanced field, and  $R_{\text{focus}}$  the radius of the laser focus.

Pettinger *et al.* observed TERS with a sharp Au tip for MGITC dye on Au(111) with a side illumination [28]. They studied the bleaching of the dye and fitted the data by taking into account the radial varying intensity distribution of the field as a Gaussian profile instead of a Heaviside profile. For the former profile, the TERS radius is smaller by a factor of  $1/2$  than for the latter profile. They obtained a TERS enhancement factor of  $6.25 \times 10^6$ . The radius of the enhanced field  $R_{\text{field}}$  is about  $50\ \text{nm}$ , which results in a TERS radius of  $25\ \text{nm}$ , which is smaller than the radius of the tip apex (about  $30\ \text{nm}$ ).

Domke *et al.* also studied the TERS of the MGITC dye on Au(111) in combination with the corresponding STM images of the probed surface region [29]. They estimated an enhancement factor of  $10^6 - 10^7$ , where five molecules should be present in the enhanced-field region, assuming an enhanced field with a radius of  $20\ \text{nm}$ , thus they claim that single-molecule Raman spectroscopy is possible. In this work, the origin of the background signal is considered to be mainly due to the adsorbate (or an adsorbate–metal complex) which most likely emits enhanced fluorescence, whereas, as a first approximation, the contribution from the substrate and contamination are negligibly small compared with resonant Raman scattering.

Wang *et al.* developed a method to prepare a sharp Au tip, as shown in Figure 1.4, and built an apparatus for Raman spectroscopy [30]. By using the original apparatus, they measured an STM image of a monolayer of 4, 4'-bipyridine (4BPY) on Au(111) as well as a TERS spectrum at the tip-approached condition. They found strong enhancement of the Raman spectrum compared to the tip-retracted condition. From the STM image, it can be seen that 4BPY is adsorbed flat on the surface, but the TERS signal seems to originate from 4BPY perpendicular to the surface.

Picardi *et al.* introduced a method to fabricate a sharp Au tip for STM by electrochemical etching [31]. The efficiency of TERS for a thin BCB dye layer using the etched sharp tip was then compared with that using an Au-coated AFM tip.

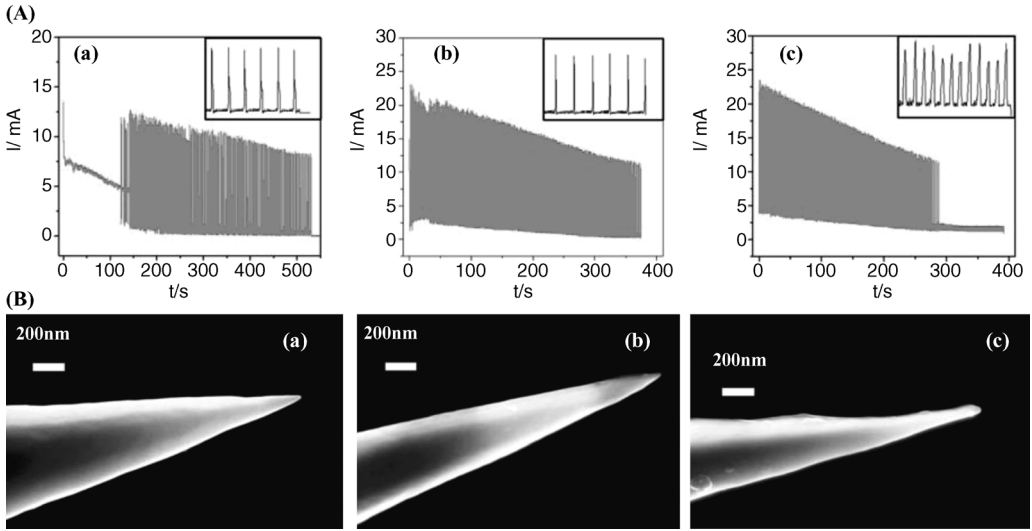


**Figure 1.4** (A) Current–time curves for Au wires etched in a mixture of HCl:ethanol (1 : 1v/v) at different voltages. (B) SEM images of the etched Au tips. A: 2.1 V, B: 2.2 V, C: 2.4 V. Reprinted with permission from Xi Wang, *Applied Physics Letters*, 91, 101105 (2007). Copyright 2007, American Institute of Physics.

A higher enhancement factor and better reproducibility were obtained when the etched sharp tip was used. This is probably due to the intrinsically lower “optical quality” of the coated tips with respect to the massive metal ones as well as to the differences in tip shapes. They calculated the Raman signal enhancement factor (EF) using the equation  $C = I_{\text{tip engaged}}/I_{\text{tip withdrawn}} = 1 + \text{EF}(\pi r_{\text{tip}}^2/A)$ , where  $C$  is the ratio of the Raman scattered intensity with the tip engaged ( $I_{\text{tip engaged}}$ ) and the tip withdrawn ( $I_{\text{tip withdrawn}}$ ),  $r_{\text{tip}}$  is the tip radius,  $A$  is the laser focal area. They estimated the EF to be about  $5 \times 10^2$  for coated AFM tips and  $4 \times 10^4$  to  $2 \times 10^5$  for etched STM tips. The same research group further studied TERS by changing the polarization of the incident laser light [32]. They measured TERS of Si(111) and BCB dye on Au(111). The experimental result with the former sample is in accord with a model reported by Ossikovski *et al.* [33]. For both samples, the TERS enhancement was larger when the incident light had an electric field component along the tip axis, while a non-negligible enhancement was also observed for the field component perpendicular to the tip axis.

We have observed the TERS of a single wall carbon nanotube (SWCNT) on highly oriented pyrolytic graphite (HOPG) [34]. The STM image and TERS image were obtained simultaneously, as shown in Figure 1.5. The TERS image was obtained by mapping the Raman signal intensity at the  $1340 \text{ cm}^{-1}$  peak (D-band) of SWCNT. An aggregate of SWCNT was observed in the STM topographical image, and strong Raman signals were observed in the TERS image. Thus, we have succeeded in observing the simultaneous spectral mapping of TERS, although the position of the SWCNT in the STM image was shifted from the TERS image by several hundred nm.

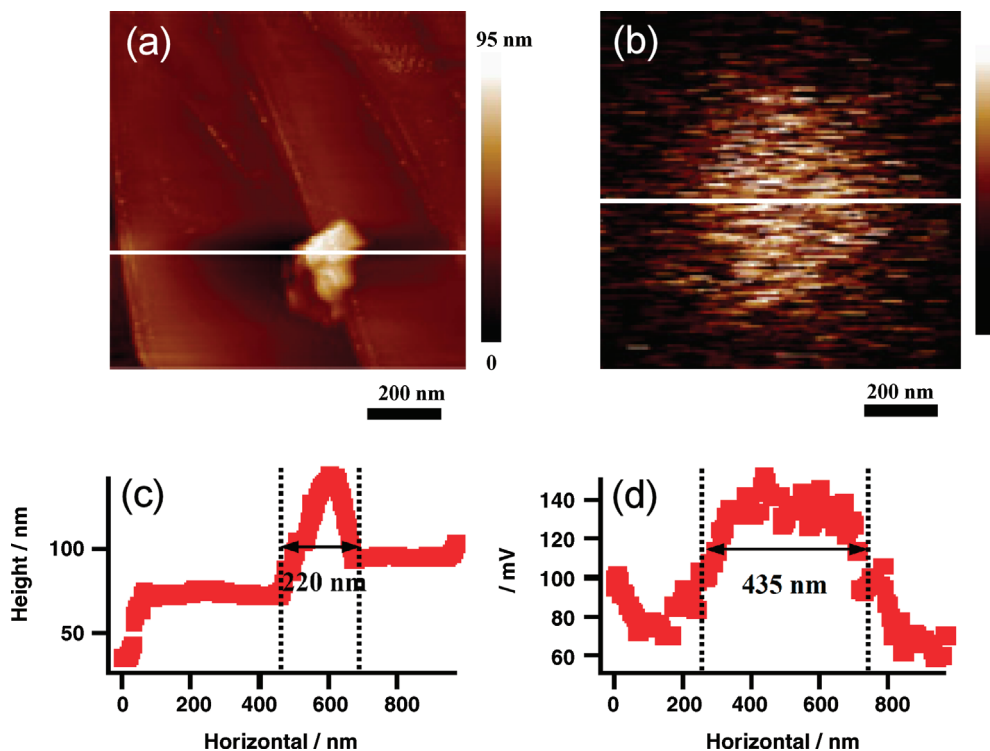


**Figure 1.5** Simultaneously obtained STM (a) and TERS (b) image of SWCNT on HOPG. The TERS image was obtained for the  $1340\text{ cm}^{-1}$  peak (D-band) of SWCNT.

This probably arises from the different position of tunneling (STM) and of field enhancement (TERS) owing to the tip shape and the height of the observation object.

#### 1.4.2

#### STM Combined With Fluorescence Spectroscopy

Anger *et al.* measured the fluorescence rate of a single Nile Blue molecule as a function of its distance from a gold nanoparticle using a scanning probe technology [35]. The fluorescence rate shows a maximum around the molecule–nanoparticle distance ( $z$ ) of 5 nm and decreases for smaller or larger  $z$ . This is due to the competition between the increased rate of excitation due to local field enhancement and the decrease in the quantum yield due to nonradiative energy transfer to the nanoparticle. They also calculated the quantum yield, excitation rate, and fluorescence rate by the multiple multipole method (MMA) and the dipole approximation. The curve of the quantum yield and fluorescence rate was reproduced only with the MMA calculation.

Kuhn *et al.* observed the fluorescence enhancement and fluorescence decay rate of a single terrylene molecule when a spherical gold nanoparticle was approached to the

molecule, using scanning probe technology [36]. The dependence of the fluorescence intensity and fluorescence decay rate on the lateral and vertical displacement of the gold nanoparticle from the molecule was measured. The fluorescence intensity was enhanced 19 times with a simultaneous 22-fold shortening of the excited state lifetime when the gold nanoparticle was in the vicinity of the molecule. The decay rates  $c_r$  (radiative decay rate),  $c_{nr}$  (nonradiative decay rate), and  $c$  (total decay rate), were calculated neglecting the effect from the substrate following a formalism presented by Puri *et al.* [37], and were compared with the experimentally obtained  $c$ . At the closest molecule–nanoparticle separation achieved experimentally, the values  $c_r = 11c_0$  and  $c_{nr} = 11c_0$  were deduced, where  $c_0$  is the unperturbed decay rate. The enhancement was larger when using an excitation wavelength near the gold nanoparticle plasmon resonance maximum wavelength than for a wavelength at the tail of the plasmon resonance, revealing the importance of the plasmon resonance in the excitation enhancement.

Nishitani *et al.* observed the tip-enhanced fluorescence of 8 nm thick meso-tetrakis (3,5-di-tertiarybutyl-phenyl)porphyrin (H2TBPP) films on ITO with an Ag tip [38]. They reported that the fluorescence was enhanced by the locally confined electromagnetic field in the vicinity of the tip. The enhancement factor is evaluated to be larger than 2000.

## 1.5 Future Prospects

We have reviewed the present situation of research on STM tip-enhanced Raman and fluorescence spectroscopy. There have been several papers showing the enhancement of Raman spectra when tips are in the approached condition. However, STM-TERS intensity mapping – scanning the tip to acquire a TERS intensity image and a STM topographical image simultaneously – seems to remain a difficult task. Very recently, Steidtner *et al.* have reported the TERS spectra and the TERS intensity mapping of a single BCB molecule on an Au(111) surface using a gold tip in ultrahigh vacuum [39]. Observation under ambient conditions is also expected for various systems.

We propose here a method to achieve single (or even sub-) molecule spectroscopy based on an additional principle to modify conventional TERS. The method utilizes the vibrational excitation of molecules by inelastic scattering of tunneling electrons, leading to further localization of the excited area. This can be applied to both fluorescence and Raman spectroscopy. For fluorescence spectroscopy, an area including the tip is illuminated with light having photon energies smaller than the absorption edge of the target molecules. When the molecule is observed by STM and electrons tunnel through the tip–molecule gap, some of the electrons are inelastically scattered and the molecule is vibrationally excited if the energy of the electron is higher than the energy of the molecular vibration. The vibrational excitation by tunneling electrons was first demonstrated by Stipe *et al.* for adsorbed single molecules under a high vacuum and at ultra-low temperature [40]. The

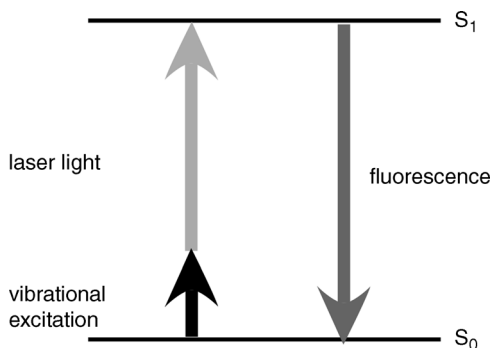


**Figure 1.6** Concept of single molecule fluorescence observation using STM.

vibrationally excited molecule can be electronically excited by the absorption of light, resulting in the emission of fluorescence. The concept of this method is presented in Figure 1.6. Because STM has an atomic scale spatial resolution, only one molecule (or part of a molecule) among other surrounding molecules can be selectively excited. Therefore, the above mentioned method would enable us to perform single (sub-) molecule fluorescence spectroscopy, even if the molecules are densely packed.

The STM tunneling current and the light intensity necessary for this method can be estimated as follows. If both the tunneling current and the light intensity are continuous with time, the probability for simultaneous injection of electron and photon will be very low. Therefore, the tunneling bias of STM and the excitation light signal should be applied as pulses in order to induce vibrational excitation and absorption of a photon simultaneously. This is shown schematically in Figure 1.7.

First we consider the electronic excitation probability  $P_{\text{elec}}$  for a single molecule during a single laser pulse. When a molecule has the absorption coefficient  $\epsilon_{\text{abs}}(\text{dm}^3 \text{mol}^{-1} \text{cm}^{-1})$ , its absorption cross section  $\sigma_{\text{abs}}$  is given by  $3.81 \times 10^{-21} \epsilon_{\text{abs}} \text{cm}^2 \text{molecule}^{-1}$ . Since the probability  $P_{\text{elec}}$  is proportional to the light intensity (photons  $\text{s}^{-1} \text{cm}^{-2}$ ) under the objective lens, it is given by

$$P_{\text{elec}} = \frac{1.91 \times 10^{-5} \epsilon_{\text{abs}} I_{\text{ph}} \lambda_{\text{ph}}}{T_{\text{ph}} \tau_{\text{ph}} S} \quad (1.1)$$

where  $I_{\text{ph}}$  (W) is the average laser power,  $T_{\text{ph}}$  (Hz) the laser repetition rate,  $\lambda_{\text{ph}}$  (nm) the laser wavelength,  $\tau_{\text{ph}}$  (s) the laser pulse width, and  $S$  ( $\text{cm}^2$ ) the illuminated area under the objective lens. For an allowed transition in typical organic molecules,  $\epsilon_{\text{abs}}$  is larger than  $10^4 \text{dm}^3 \text{mol}^{-1} \text{cm}^{-1}$ , and a conventional table-top ps laser can safely emit  $1 \mu\text{W}$  green light ( $\lambda_{\text{ph}} = 500 \text{nm}$ ) with a repetition rate of 10 MHz. Assuming that the illuminated area under the objective lens is  $100 \mu\text{m}$  in diameter, we obtain  $P_{\text{elec}} = 1.2 \times 10^5$ . This means that the molecule under the microscope can be definitely excited during a short ps pulse.

The next step is to estimate how long a molecule can stay in its vibrational excited state during a single electric pulse. A conventional electronic circuit cannot generate a short pulse like 10 ps, so that the use of electric pulses longer than 100 ps is more

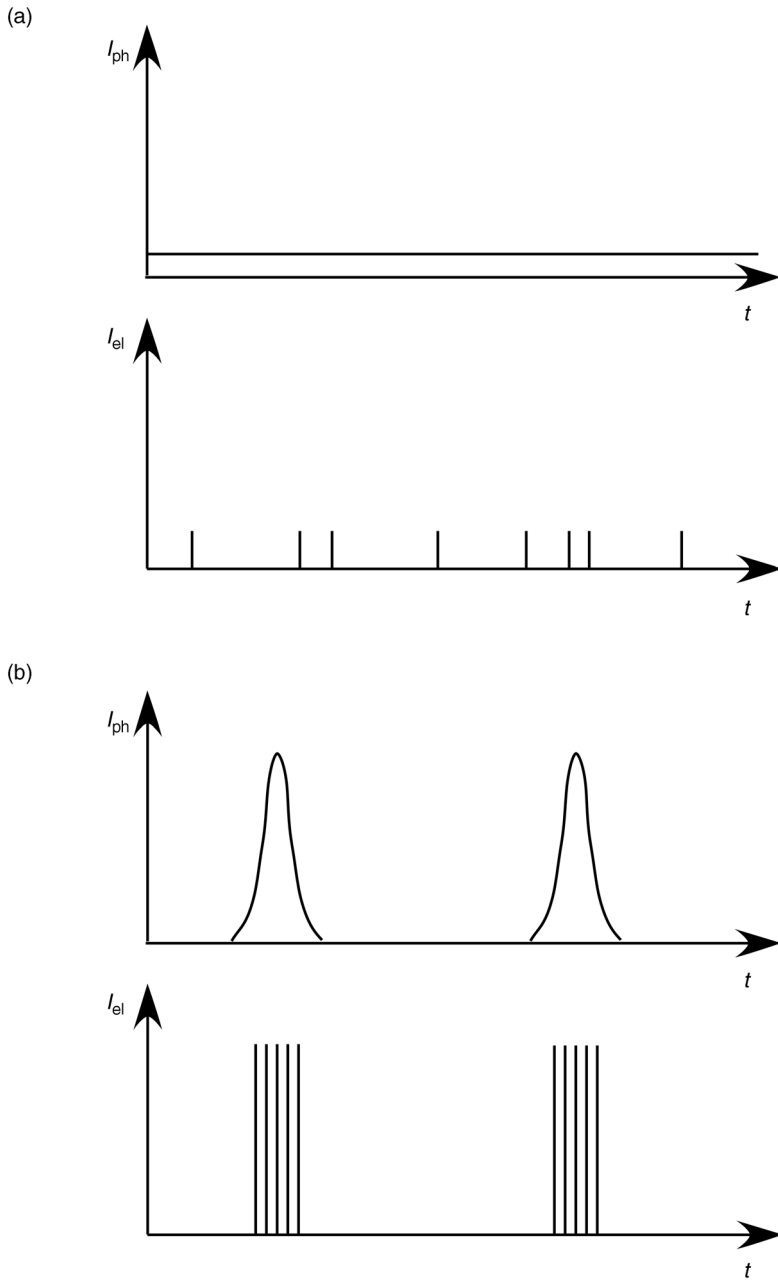


**Figure 1.7** Schematics of simultaneous incoming probability of electrons and photons for (a) continuous mode and (b) pulsed mode.

realistic. The lifetime of vibrational excited states in organic molecules is generally in the range of 10 ps, which means that the molecule can relax immediately and be excited again during the electric pulses. The average dwelling time for the molecule in its vibrational excited states during a single electric pulse is given by

$$T_{\text{dwell}} = \frac{6.25 \times 10^9 \eta_{\text{el}} I_{\text{el}} \tau_{\text{vib}}}{T_{\text{el}}} \quad (1.2)$$

where  $\eta_{\text{el}}$  denotes the probability for vibrational excitation by a single electron,  $I_{\text{el}}$  (nA) average tunneling current,  $\tau_{\text{vib}}$  (s) the lifetime of vibrational excited states,  $T_{\text{el}}$  (Hz) the tunneling bias repetition rate. Stipe *et al.* reported that the total conductance increase induced by inelastic electron tunneling for acetylene molecules is of the order of several percent [40]. Therefore, several percent of the electrons injected into the molecule are considered to induce vibrational excitation, although this is dependent on the molecule, its vibrational mode, and other surrounding conditions. By assuming  $\eta_{\text{el}} = 1\%$ ,  $I_{\text{el}} = 1$  nA,  $\tau_{\text{vib}} = 10$  ps, and  $T_{\text{el}} = 10$  MHz, we obtain  $T_{\text{dwell}} = 62.5$  ps. If we can utilize electric pulses shorter than this time duration as well as synchronized with the light pulses, we would be able to further excite the molecule in its vibrationally excited state to the electronically excited states. Of course, the values of the above variables depend on each experimental system, and optimization of the values will be necessary.

For Raman spectroscopy, the experimental set-up is similar to that for fluorescence spectroscopy, but the observation wavelength should be in the range of anti-Stokes Raman spectra. When a molecule is excited vibrationally with pulsed tunneling currents, the molecule is expected to emit anti-Stokes scattered light when the probe light pulses are synchronized. In general, Raman scattering efficiency is lower than that of fluorescence, meaning that the anti-Stokes Raman measurement may be difficult. In any case, the key is how to increase the dwelling time for a molecule in its vibrationally excited states.

In summary, recent progress and future prospects in the research field of fluorescence and Raman spectroscopy combined with STM in order to achieve high spatial resolution spectroscopy have been reviewed. In the near future, single (sub-) molecule STM spectroscopy is expected to be applied to the nano-world of science and engineering.

## References

- 1 Imura, K. and Okamoto, H. (2008) Development of novel near-field microspectroscopy and imaging of local excitations and wave functions of nanomaterials. *Bull. Chem. Soc. Jpn.*, **81**, 659–675.
- 2 Anderson, N., Hartschuh, A., Cronin, S. and Novotny, L. (2005) Nanoscale vibrational analysis of single-walled carbon nanotubes. *J. Am. Chem. Soc.*, **127**, 2533–2537.
- 3 Binnig, G., Rohrer, H., Gerber, Ch. and Weibel, W. (1982) Surface studies by scanning tunneling microscopy. *Phys. Rev. Lett.*, **49**, 57–61.
- 4 Bai, C. (2000) *Scanning Tunneling Microscopy and Its Applications*, (Springer

- Series in Surface Sciences*), 2nd Revised edn, Springer, New York.
- 5 Julian Chen, C. (2008) *Introduction to Scanning Tunneling Microscopy*, 2nd edn, (Monographs on the Physics and Chemistry of Materials) (64), Oxford University Press, Oxford.
  - 6 Moskovits, M. (1985) Surface-enhanced spectroscopy. *Rev. Mod. Phys.*, **57**, 783–826.
  - 7 Champion, A. and Kambhampati, P. (1998) Surface-enhanced Raman scattering. *Chem. Soc. Rev.*, **27**, 241–250.
  - 8 Shen, C. K., Heinz, T. H., Ricard, D. and Shen, Y. R. (1983) Surface-enhanced second-harmonic generation and Raman scattering. *Phys. Rev. B*, **27**, 1965–1979.
  - 9 Barber, P. W., Chang, R. K. and Massoudi, H. (1983) Surface-enhanced electric intensities on large silver spheroids. *Phys. Rev. Lett.*, **50**, 997–1000.
  - 10 Bohren, C. F. and Huffman, D. R. (2004) *Absorption and Scattering of Light by Small Particles*, Wiley-VCH, Weinheim.
  - 11 Kottmann, J. P., Martin, O. J. F., Smith, D. R. and Schultz, S. (2000) Spectral response of plasmon resonant nanoparticles with a non-regular shape. *Opt. Express*, **6**, 213–219.
  - 12 Purcell, E. M. and Pennypacker, C. R. (1973) Scattering and absorption of light by non-spherical dielectric grains. *Astrophys. J.*, **186**, 705–714.
  - 13 Draine, B. T. and Flatau, P. J. (1994) Discrete-dipole approximation for scattering calculations. *J. Opt. Soc. Am. A*, **11**, 1491–1499.
  - 14 Jeanmaire, D. L. and Van Duyne, R. P. (1977) Surface Raman spectroelectrochemistry: Part I. Heterocyclic, aromatic, and aliphatic amines adsorbed on the anodized silver electrode. *J. Electroanal. Chem.*, **84**, 1–20.
  - 15 Nie, S. and Emory, S. R. (1997) Probing single molecules and single nanoparticles by surface-enhanced Raman scattering. *Science*, **275**, 1102–1106.
  - 16 Neacsu, C. C., Dreyer, J., Behr, N. and Raschke, M. B. (2006) Scanning-probe Raman spectroscopy with single-molecule sensitivity. *Phys. Rev. B*, **73**, 193406-1–193406-4.
  - 17 Demming, F., Jersch, J., Dickmann, K. and Geshev, P. I. (1998) Calculation of the field enhancement on laser-illuminated scanning probe tips by the boundary element method. *Appl. Phys. B*, **66**, 593–598.
  - 18 Jersch, J., Demming, F., Hildenhagen, L. J. and Dickmann, K. (1998) Field enhancement of optical radiation in the nearfield of scanning probe microscope tips. *Appl. Phys. A*, **66**, 29–34.
  - 19 Mills, D. L. (2002) Theory of STM-induced enhancement of dynamic dipole moments on crystal surfaces. *Phys. Rev. B*, **65**, 125419-1–125419-11.
  - 20 Wu, S. and Mills, D. L. (2002) STM-induced enhancement of dynamic dipole moments on crystal surfaces: theory of the lateral resolution. *Phys. Rev. B*, **65**, 205420-1–205420-7.
  - 21 Rendell, R., Scalapino, D. and Mühlischlegel, B. (1978) Role of local plasmon modes in light emission from small-particle tunnel junctions. *Phys. Rev. Lett.*, **41**, 1746–1750.
  - 22 Klein, S., Geshev, P., Witting, T., Dickmann, K. and Hietschold, M. (2003) Enhanced Raman scattering in the near field of a scanning tunneling tip – an approach to single molecule Raman spectroscopy. *Electrochemistry*, **71**, 114–116.
  - 23 Pettinger, B., Picardi, G., Schuster, R. and Ertl, G. (2000) Surface enhanced Raman spectroscopy: towards single molecule spectroscopy. *Electrochemistry*, **68**, 942–949.
  - 24 Downes, A., Salter, D. and Elfick, A. (2006) Finite element simulations of tip-enhanced Raman and fluorescence spectroscopy. *J. Phys. Chem. B*, **110**, 6692–6698.
  - 25 Pettinger, B., Picardi, G., Schuster, R. and Ertl, G. (2002) Surface-enhanced and STM-Tip-enhanced Raman spectroscopy at metal surfaces. *Single Mol.*, **5–6**, 285–294.

- 26 Pettinger, B., Picardi, G., Schuster, R. and Ertl, G. (2003) Surface-enhanced and STM tip-enhanced Raman spectroscopy of  $\text{CN}^-$  ions at gold surfaces. *J. Electroanal. Chem.*, **554**, 293–299.
- 27 Ren, B., Picardi, G. and Pettinger, B. (2004) Preparation of gold tips suitable for tip-enhanced Raman spectroscopy and light emission by electrochemical etching. *Rev. Sci. Instrum.*, **75**, 837–841.
- 28 Pettinger, B., Ren, B., Picardi, G., Schuster, R. and Ertl, G. (2005) Tip-Enhanced Raman spectroscopy (TERS) of malachite green isothiocyanate at Au(111): bleaching behavior under the influence of high electromagnetic fields. *J. Raman Spectrosc.*, **36**, 541–550.
- 29 Domke, K. F., Zhang, D. and Pettinger, B. (2006) Toward Raman fingerprints of single dye molecules at atomically smooth Au(111). *J. Am. Chem. Soc.*, **128**, 14721–14727.
- 30 Wang, X., Liu, Z., Zhuang, M.-D., Zhang, H.-M., Wang, X., Xie, Z.-X., Wu, D.-Y., Ren, B. and Tian, Z.-Q. (2007) Tip-enhanced Raman spectroscopy for investigating adsorbed species on a single-crystal surface using electrochemically prepared Au tips. *Appl. Phys. Lett.*, **91**, 101105–101105-3.
- 31 Picardi, G., Nguyen, Q., Schreiber, J. and Ossikovski, R. (2007) Comparative study of atomic force mode and tunneling mode tip-enhanced Raman spectroscopy. *Eur. Phys. J. Appl. Phys.*, **40**, 197–201.
- 32 Picardi, G., Nguyen, Q., Ossikovski, R. and Schreiber, J. (2007) Polarization properties of oblique incidence scanning tunneling microscopy – tip-enhanced Raman spectroscopy. *Appl. Spectrosc.*, **61**, 1301–1305.
- 33 Ossikovski, R., Nguyen, Q. and Picardi, G. (2007) Simple model for the polarization effects in tip-enhanced Raman spectroscopy. *Phys. Rev. B*, **75**, 045412-1–045412-9.
- 34 Yoshidome, M. (2006) Study of molecular aggregates on solid surface using scanning tunneling microscopy and Raman spectroscopy, Ph.D. thesis, Tohoku University.
- 35 Anger, P., Bharadwaj, P. and Novotny, L. (2006) Enhancement and quenching of single-molecule fluorescence. *Phys. Rev. Lett.*, **96**, 113002-1–113002-4.
- 36 Kühn, S., Håkanson, U., Rogobete, L. and Sandoghdar, V. (2006) Enhancement of single-molecule fluorescence using a gold nanoparticle as an optical nanoantenna. *Phys. Rev. Lett.*, **97**, 017402-1–017402-4.
- 37 Das, P. C. and Puri, A. (2002) Energy flow and fluorescence near a small metal particle. *Phys. Rev. B*, **65**, 155416-1–155416-8.
- 38 Nishitani, R., Liu, H. W., Kasuya, A., Miyahira, H., Kawahara, T. and Iwasaki, H. (2007) STM Tip-enhanced photoluminescence from porphyrin film. *Surf. Sci.*, **601**, 3601–3604.
- 39 Steidtner, J. and Pettinger, B. (2008) Tip-enhanced Raman spectroscopy and microscopy on single dye molecules with 15 nm resolution. *Phys. Rev. Lett.*, **100**, 236101-1–236101-4.
- 40 Stipe, B. C., Rezaei, M. A. and Ho, W. (1998) Single-molecule vibrational spectroscopy and microscopy. *Science*, **280**, 1732–1735.